Glaucoma

Neuroprotective Gene Therapy by Overexpression of the Transcription Factor MAX in Rat Models of Glaucomatous Neurodegeneration

Rafael Lani-Louzada,[1] Camila Marra,[1] Mariana Santana Dias,[1] Victor Guedes de Araújo,[1] Carla Andreia Abreu,[1] Vinícius Toledo Ribas,[2] Daniel Adesse,[3] Silvana Allodi,[4] Vince Chiodo,[5] William Hauswirth,[5] Hilda Petrs-Silva,[1] and Rafael Linden[1]

[1]Laboratory of Neurogenesis, Carlos Chagas Filho Institute of Biophysics, Universidade Federal do Rio de Janeiro, Rio de Janeiro, Brazil
[2]Laboratory of Neurobiology, Department of Morphology, Institute of Biological Sciences, Universidade Federal de Minas Gerais, Belo Horizonte, Brazil
[3]Laboratory of Structural Biology, Oswaldo Cruz Institute, FIOCRUZ, Rio de Janeiro, Brazil
[4]Laboratory of Comparative and Developmental Neurobiology, Carlos Chagas Filho Institute of Biophysics, Universidade Federal do Rio de Janeiro, Rio de Janeiro, Brazil
[5]Department of Ophthalmology, University of Florida, Gainesville, Florida, United States

Correspondence: Rafael Linden, Instituto de Biofísica Carlos Chagas Filho, Universidade Federal do Rio de Janeiro, Rio de Janeiro 21941-901, Brazil; rlinden@biof.ufrj.br.
Hilda Petrs-Silva, Instituto de Biofísica Carlos Chagas Filho, Universidade Federal do Rio de Janeiro, Rio de Janeiro 21941- 901, Brazil; hilda@biof.ufrj.br.

Received: August 27, 2021
Accepted: January 3, 2022
Published: February 1, 2022

Citation: Lani-Louzada R, Marra C, Dias MS, et al. Neuroprotective gene therapy by overexpression of the transcription factor MAX in rat models of glaucomatous neurodegeneration. *Invest Ophthalmol Vis Sci.* 2022;63(2):5. https://doi.org/10.1167/iovs.63.2.5

Purpose. Based on our preview evidence that reduced nuclear content of the transcription factor Myc-associated protein X (MAX) is an early event associated with degeneration of retinal ganglion cells (RGCs), in the present study, our purpose was to test whether the overexpression of human MAX had a neuroprotective effect against RGC injury.

Methods. Overexpression of either MAX or green fluorescent protein (GFP) in the retina was achieved by intravitreal injections of recombinant adenovirus-associated viruses (rAAVs). Lister Hooded rats were used in three models of RGC degeneration: (1) cultures of retinal explants for 30 hours ex vivo from the eyes of 14-day-old rats that had received intravitreal injections of rAAV2-*MAX* or the control vector rAAV2-*GFP* at birth; (2) an optic nerve crush model, in which 1-month-old rats received intravitreal injection of either rAAV2-*MAX* or rAAV2-*GFP* and, 4 weeks later, were operated on; and (3) an ocular hypertension (OHT) glaucoma model, in which 1-month-old rats received intravitreal injection of either rAAV2-*MAX* or rAAV2-*GFP* and, 4 weeks later, were subject to cauterization of the limbal plexus. Cell death was estimated by detection of pyknotic nuclei and TUNEL technique and correlated with MAX immunocontent in an ex vivo model of retinal explants. MAX expression was detected by quantitative RT-PCR. In the OHT model, survival of RGCs was quantified by retrograde labeling with DiI or immunostaining for BRN3a at 14 days after in vivo injury. Functional integrity of RGCs was analyzed through pattern electroretinography, and damage to the optic nerve was examined in semithin sections.

Results. In all three models of RGC insult, gene therapy by overexpression of MAX prevented RGC death. Also, ON degeneration and electrophysiologic deficits were prevented in the OHT model.

Conclusions. Our experiments offer proof of concept for a novel neuroprotective gene therapy for glaucomatous neurodegeneration based on overexpression of MAX.

Keywords: glaucomatous neurodegeneration, MAX overexpression, adeno-associated viral vectors, intravitreal injection, neuroprotection

Loss of retinal ganglion cells (RGCs) and degeneration of the optic nerve are the final common events that lead to vision impairment in glaucoma and other optic neuropathies.[1–3] Those insults originate from negative changes of the cellular and molecular environment that impair cell survival capacity.[4–6] Among optic neuropathies, glaucoma is the most prevalent and is the second leading cause of blindness worldwide.[7,8] Elevated intraocular pressure (IOP) is the most important risk factor and, so far, the only therapeutic target for the treatment of glaucoma, but degeneration of RGCs often proceeds despite successful lowering of the IOP.[9,10] This scenario calls for novel approaches, such as neuroprotective strategies aimed at either preventing or retarding the degeneration of RGCs.[11]

Vision ranks among the most frequent areas of clinical application of gene therapy.[12,13] However, to target nonmonogenic neurodegenerative diseases such as glaucoma, strategies have focused primarily on

Copyright 2022 The Authors

This work is licensed under a Creative Commons Attribution-NonCommercial-NoDerivatives 4.0 International License.

Downloaded from hwmaint.iovs.org on 04/25/2024

neuroprotection, which aims at slowing or preventing the loss of RGCs by altering their physiology. Most cases of glaucoma have an unclear, heterogeneous etiology involving multiple genetic and environmental risk factors,[14,15] all of which converge to regulate cell death of RGCs in both experimental[16] and human glaucoma.[17] For these reasons, gene therapy for adult-onset glaucoma has been primarily approached in two ways: (1) by enhancing the activity of innate survival pathways of RGCs or (2) by inhibiting their progression to cell death. For example, overexpression of neurotrophic factors, such as BDNF,[18] FGF,[19] CNTF,[20] GDNF,[21] and PEDF,[22] have been tested for neuroprotective gene therapy, and several such molecules either delayed or protected RGC degeneration in animal models of glaucoma. However, limited long-term effectiveness of the increased content of neurotrophic factors led to diminished neuroprotective response, in addition to the risk of oncogenic activity of the cognate neurotrophic receptors.[23–26] Alternative approaches explored the therapeutic potential of proteins to counteract the apoptotic machinery itself, such as BAG1,[27] BCL-XL,[28] XIAP,[29] and sFasL.[30] However, downregulation of the apoptotic machinery is oncogenic, and overexpression of transgenes blocking the apoptotic machinery has been causatively related to various types of cancers.[31,32] Recently, immunomodulation blocking C3 was successfully used to subvert the degenerative environment in experimental glaucoma,[33] but a therapeutic approach based on one-shot gene therapy has yet to provide permanent beneficial outcomes.

MYC-associated protein X (MAX) is a ubiquitous, constitutively expressed transcription factor that plays a central role in the control of the MYC/MXD axis, in which the deregulation contributes to the genesis of many human cancers.[34] *MAX* is a tumor-suppressor gene[35,36] and is the only member of the network that homodimerizes efficiently upon overexpression, although the biological role of such dimers remains unknown. Studies in *Drosophila* suggested that the pivotal role of MAX is related more to transcription repression than activation.[37] MAX is ubiquitously expressed, and its germline deletion in mice leads to embryonic lethality.[38] Recently MAX appeared, among a set of 25 transcription factors, as the strongest contributor to gene expression in various human brain regions,[39] which supports its relevance to gene regulation in nervous tissue.

With the use of retinal explants as a model to investigate mechanisms of cell death, we previously showed that MAX is found primarily within the nucleus of normal RGCs and disappears from the nucleus early upon induction of programmed cell death, in advance of both DNA fragmentation and chromatin condensation.[40,41] These data were in line with evidence that selective overexpression of MAX in endothelial cells blocks apoptosis promoted by serum withdrawal[42] and raised the hypothesis that the reduced nuclear content of MAX might be instrumental for the degeneration of the RGCs. Indeed, an ex vivo study of axotomized retinal explants[43] showed that condensed TUNEL-positive nuclei of RGCs did not express MAX, while RGCs overexpressing MAX showed healthy morphology.

In the present study, we tested the neuroprotective effect of rAAV2-*MAX* ex vivo and extended our study of neuroprotection to in vivo rat models of RGC degeneration, induced either by optic nerve crush (ONC) or by an ocular hypertension (OHT) model of limbal plexus cautery.[44] Our results provide proof of principle for rAAV2-*MAX* as a tool for neuroprotective gene therapy in glaucoma through prevention of RGC degeneration and preservation of optic nerve axons.

Methods

Animal Handling

Male and female Lister Hooded rats were bred and housed in the animal facility at the Federal University of Rio de Janeiro, in plastic cages, under a 12-hour light/dark cycle, with water and food ad libitum. All experiments were carried out in agreement with the ARVO Statement for the Use of Animals in Ophthalmic and Vision Research, and the protocol was approved by the Institutional Animal Experimentation Ethics Committee (UFRJ 01200.001568/2013-87).

Vector Production

All rAAV2 vector preparations were done by a double transfection protocol as previously described.[45] Crude iodixanol fractions of rAAV2 vector were further purified and concentrated by chromatography on a 5-mL HiTrap Q Sepharose column using an AKTA FPLC system (Amersham Biosciences, Piscataway, NJ, USA). Vectors were eluted from the column using 215 mM NaCl, pH 8.0, and the vector-containing fractions collected, pooled, concentrated, and buffer exchanged into Alcon BSS with 0.014% Tween 20, using a Biomax 100 K concentrator (Millipore, Burlington, MA, USA). The titer of DNase-resistant vector genomes was measured by real-time PCR relative to a standard. Finally, the purity of the vector was validated by silver-stained sodium dodecyl sulfate–polyacrylamide gel electrophoresis, assayed for sterility and lack of endotoxin, and then aliquoted and stored at −80°C. Vectors contained the sequences encoding either humanized green fluorescent protein (h*GFP*)[46] or human *MAX* under the control of the ubiquitous citomegalovirus (CMV) enhancer/chicken β-actin (CBA) promoter and simian virus 40 late polyadenylation signal (polyA).

For Ex Vivo Experiments

Intravitreal Injections. Intravitreal injection of rAAV2 vector was performed 2 weeks before retinal explants, as previously described.[43] In 1-day-old (P1) rat pups, hypothermia was used to induce anesthesia. Pups were placed onto a dry rubber glove set on ice for 2 to 3 minutes and then placed onto a clean paper towel under the dissecting scope. The skin was cleaned with Betadine (Cristalia, São Paulo, Brazil) and then cut where the future eyelid develops. The skin was gently pushed away with a pair of sterile forceps to expose the eyeball. Injection of 1 µL containing 10^9 vg/µL of the vector was made directly into the eyeball with a 33-gauge needle (10 mm, pst3) fit in a 5-µL syringe (#65RN; Hamilton, Reno, NV, USA). Injections were given slowly over 20 seconds, and no leakage was noticed. The eyelid was gently closed and covered with oxytetracycline ointment (Cristalia), and then pups were placed on a warm heating mat until fully recovered and returned to the mother.

Preparation of Explants and Histology. Two weeks after intravitreal injection of rAAV2, at 15 days after birth, retinal explants were prepared as previously described.[43] Rats were euthanized, and the eyeballs were removed and collected in an ice-cold PBS solution containing 1% penicillin. The anterior segment was removed by a

Investigative Ophthalmology & Visual Science

Downloaded from hwmaint.iovs.org on 04/25/2024

sharp incision in the pars plana and cut 360°. The retina was gently dissected from the pigment epithelium with microforceps and Vannas scissor and cut out at the optic nerve head. Fragments of about 2 mm in size were cut and placed in 25-mL tight-lidded Erlenmeyer flasks containing 5 mL Dulbecco's modified Eagle's medium supplemented with 5% fetal bovine serum, 2 mM glutamine, 20 mM Hepes, 10 U/mL penicillin, and 100 µg/mL streptomycin, all at pH 7.4 (Thermo Fisher, Rockford, IL, USA). The tissue fragments were incubated at 37°C in an atmosphere of 5% CO_2 and 95% air, in an orbital shaker at 80 to 90 rpm for 30 hours. For histologic and histochemical analyses, the tissue was fixed by immersion in 4% paraformaldehyde in sodium phosphate buffer (PBS), pH 7.4, for 2 hours and then cryoprotected in 30% (w/v) sucrose in phosphate buffer. The explants were oriented under a dissecting microscope in an aluminum chamber filled with Tissue-Tek optimal cutting temperature (OCT) embedding medium (Sakura, Torrance, CA, USA) and frozen in liquid nitrogen, and 10-µm-thick transverse sections were cut in a cryostat. Sections were mounted and stained with neutral red.

Detection of Apoptotic Cells and Immunolabeling of Tissue Slices. After 30 hours in vitro, cell death was detected either by the chromatin condensation (pyknosis) stained with neutral red or with the DeadEnd Fluorometric TUNEL System (Promega, Madison, MI, USA) used according to the manufacturer's protocol. Briefly, sections were permeabilized with 0.5% Triton X-100 in PBS for 5 minutes, washed, and incubated for 60 minutes at 37°C with TdT reaction mixture, and the reaction was stopped by washing with 1× PBS. For immunohistochemistry, sections were incubated with 0.5% Triton X-100 for 15 minutes, then washed three times with PBS for 5 minutes each, followed by incubation with a blocking solution of 1% bovine serum albumin for 30 minutes. The sections were incubated with anti-MAX (rabbit polyclonal IgG 1:100, #SC-197; Santa Cruz Biotechnology, Santa Cruz, CA, USA) and anti–β-III-tubulin (TUJ-1; mouse monoclonal IgG 1:500, #MMS-435P; Covance, Princeton, NJ, USA), overnight at 4°C, followed by incubation with secondary antibodies (1:400) anti-rabbit IgG Alexa-Fluor 555, rabbit IgG Alexa-Fluor 647, and anti-mouse IgG Alexa-Fluor 488 (Molecular Probes, Eugene, OR, USA) for 2 hours at room temperature. All results were examined in an epifluorescence confocal LSM-510META microscope (Carl Zeiss, Göttingen, Germany), and to compare transduction efficiency by anti-MAX fluorescence intensity, images of the retina sections were taken with fixed acquisition and orientation parameters.

For In Vivo Experiments

Intravitreal Injection. Intravitreal injection of rAAV2 vector was performed as described before,[47] at 4 weeks before RGC crush and OHT. Thirty-day-old young adult rats were anesthetized by intraperitoneal injection of a mixture of ketamine (75 mg/kg) and xylazine (5 mg/kg) (Cristalia). Prior to intravitreal injections, animals received eye drops of tropicamide 1% and proxymetacaine hydrochloride 0.5% (Anestalcon; Novartis Biociências S.A., São Paulo, Brazil). An incision was made in the pars plana of the sclera in the superior-temporal site using a 33-gauge needle, and injections were carried out as above, at a volume of 3 µL containing 10^9 vg/µL. After injection(s), retinal integrity was verified by ocular fundus examination, and then oxytetracycline ointment was topically applied.

Real-Time PCR. Retinas of adult rats, 4 weeks after rAAV2-*MAX* transduction, as well as retinas from uninjected eyes, were lysed using Trizol reagent (Invitrogen, Carlsbad, CA, USA), and total RNA was extracted following the instructions of the manufacturer. DNA was eliminated with a DNA-free Kit (Ambion, Austin, TX, USA) for 10 minutes at 37°C, followed by precipitation with 3 mM sodium acetate/ethanol and resuspension in diethylpyrocarbonate (DEPC)-treated water. Nanodrop (Thermo Fisher, Rockford, IL) was used to define the purity and amount of RNA in samples. One microgram of RNA was used to synthetize cDNA using the First-Strand cDNA Synthesis Kit (GE Healthcare, Chicago, IL, USA). cDNA was amplified in a 25-µL real-time PCR reaction containing 12.5 µL SYBR Green, 0.5 µL diluted cDNA (1:3), and 200 nM of each commercial primer (GGID: PPH00190A-200 human *MAX* and GGID: PPR06557B-200; cat. 330001, Qiagen, Germantown, MD, USA). The $2^{-\Delta\Delta Ct}$ method was used to determine relative expression normalized to *Gapdh* mRNA levels. Four biological replicates were analyzed in technical triplicates.

Retrograde Tracing for Optic Nerve Crush Experiments. 1,1′-Dioctadecyl-3,3,3′,3′-tetramethylindocarbocyanine (DiI) was bilaterally injected into the superior colliculi (SCs) of 5-day-old rats, which led to the labeling of virtually all the RGCs.[48,49] Rat pups were anaesthetized on ice. Under a stereoscopic microscope (Carl Zeiss), the skull was exposed; a small bone aperture was made to expose the underlying SCs. Three 0.1-mL injections of DiI (10% in dimethyl formamide) (Invitrogen) were then made into the left SC using a Hamilton syringe (series 7000; ref. 86257, pst 3).

Optic Nerve Crush. Two-month-old rats, previously subjected to retrograde tracing with DiI and at 1 month after rAAV2 injection or uninjected, were deeply anesthetized by intraperitoneal injection of a mixture of xylazine (10 mg/kg body weight [BW]) and ketamine (60 mg/kg BW). Under a stereoscopic microscope, the right optic nerve was accessed through an incision made in the superior orbital rim, and the conjunctiva was dissected with forceps toward the back of the eye to expose the retrobulbar portion of the optic nerve. The optic nerve was completely crushed for 10 seconds at 3 mm from the optic disc, using a pair of watchmaker's forceps. Sham-operated rats underwent the same procedure, except that the forceps were not closed. Animals were euthanized 2 weeks after the procedure.

Ocular Hypertension. The procedure followed the protocol described in Lani et al.[44] Briefly, rats at 2 months old were deeply anesthetized with an intramuscular injection of ketamine hydrochloride (75 mg/kg) and xylazine hydrochloride (5 mg/kg), as well as topical eye anesthesia with proxymetacaine hydrochloride 0.5%. A low-temperature ophthalmic cautery (Bovie Medical Corporation, Clearwater, FL, USA) was used to cauterize the limbal plexus in a 360° ring around the cornea, visualized through a stereomicroscope at 40× magnification. Care was taken not to compromise the periphery of the cornea. After surgery, a drop of ophthalmic prednisolone acetate (10 mg/mL; Cristalia) was applied and maintained in contact with the anterior surface of the right eye during approximately 40 seconds, after which it was replaced by an ophthalmic ointment of antibiotics (oxytetracycline hydrochloride 30 mg/g and polymyxin B 10.000 U/g; Cristalia). IOP was measured using a handheld tonometer (TonoLab; Icare, Vantaa, Finland, Canada). Measurements were done immediately before and after the surgical procedure and then

Investigative Ophthalmology & Visual Science

Downloaded from hwmaint.iovs.org on 04/25/2024

every day in the morning up to 14 days after surgery with rats lightly anesthetized (ketamine: 18.75 mg/kg; xylazine: 1.25 mg/kg).

Pattern Electroretinogram in OHT Experiments. The procedure followed the protocol described in Lani et al.[44] The cornea was topically anesthetized with a drop of proxymetacaine hydrochloride 0.5%, and the active electrode (a stainless-steel needle 0.25 × 15 mm; Hansol Medical Co., Seoul, Republic of Korea) was inserted carefully at the temporal periphery of the transitional zone. The reference and ground electrodes were stainless-steel needles (0.4 × 37 mm; Chalgren Enterprises, Gilroy, CA, USA), positioned subcutaneously into the ipsilateral temporal canthus and the left hindlimb, respectively. The steady-state pattern electroretinogram (PERG) amplitude gathered the component of the wave most likely associated with the RGC bioelectrical response (negative deflection N2 of the transient-state PERG), generating a stable and reproducible sinusoid. The stimulus consisted of contrast reversal of a checkerboard with black and white squares alternating at 15 reversals/s, with constant average luminance (250 cd/m^2), and presented on an LCD monitor (23 in.; model LS23B550, Samsung Electronics Co., Ltd., Seoul, Republic of Korea) positioned at 20 cm from the examined eye. The band-pass filter was set to 1 to 100 Hz, and signals were averaged 200 to 300 times to eliminate noise. Six distinct spatial frequencies were presented, in the following order, for all animals: 0.018, 0.585, 0.073, 0.037, 0.292, and 0.146 cycles/deg. The amplitude of the stored sinusoidal waveforms was analyzed using a custom-made Fast Fourier Transform (FFT) algorithm programmed through MATLAB language (The MathWorks, Natick, MA, USA).

Flat-Mount Dissection and Immunolabeling. Upon dissection of the eyeballs, retinas in PBS were dissected so that tissue topographic orientation was preserved, using the nasal caruncle and the choroid fissure as landmarks.[50] Retinas were flattened with the vitreous side up as flat-mounts by making four radial cuts, followed by fixation with 4% paraformaldehyde for 15 minutes at room temperature. Retinas of ONC that were retrolabeled with DiI were washed three times with PBS and counterstained with Sytox Green (Thermo Fisher) to visualize cell nuclei, then covered with antifading mounting media. Retinas of OHT were immunolabeled with an anti-Brn3a primary antibody (goat polyclonal IgG, sc-31984; Santa Cruz Biotechnology; 1:1000 diluted in PBS 1× + BSA 0.1%), followed by a donkey anti-goat polyclonal IgG secondary antibody, conjugated with Alexa Fluor 555 (2 mg/mL, A21432; Thermo Fisher Scientific; 1:1000 diluted in PBS 1× + BSA 0.1%), at room temperature (RT). DAPI (4′,6-diamidino-2-phenylindole; Invitrogen) was used for nuclear staining (10 minutes, at RT). The retinas were then flat-mounted in glass slides with the vitreous side up and coverslipped in antifade mounting medium (#S3023; DAKO, Agilent Technologies, Santa Clara, CA, USA).

Image Acquisition and Processing. Photomicrographs were taken in an epifluorescence confocal microscope LSM 510META (Carl Zeiss), with the experimenter blinded to the sample treatments. To estimate cell densities, 32 photos were taken of the whole retina under a Plan-Neofluar 40×/1.3 objective (NA = 0.5). For each quadrant of the retina, 8 photos were taken, of which 2 were from central retina (~0.9 mm from optic disc), 3 from mid-retina (~2.0 mm from optic disc), and 3 from peripheral retina (~3.7 mm from optic disc), for a total of 32 photos per retina. Average cell counts were divided by the field area. A blinded experimenter used ImageJ (FIJI) version 2.0 (Wayne Rasband, National Institutes of Health [NIH], Bethesda, MD, USA) software to carry out all image processing.

Processing of the Optic Nerve for Semithin Sections. Following euthanasia and ocular enucleation, 2-mm-long segments of the optic nerve at 1 mm distal from the eye were fixed by immersion in 2.5% glutaraldehyde for 2 hours, washed in 0.1 M cacodylate buffer (pH 7.4), and postfixed for 1 hour in 1% osmium tetroxide containing 0.8% potassium ferrocyanide and 5 nM calcium chloride in 0.1 M cacodylate buffer (pH 7.4). The segments were rinsed in 0.1 M cacodylate buffer (pH 7.4) and distilled water and block-stained in 1% uranyl acetate overnight, dehydrated in a graded acetone series, embedded in Polybed 812 resin (Polysciences, Warrington, PA, USA), and polymerized at 60°C for 48 hours.

Morphometric Analysis of the Optic Nerve. Semithin (500 nm) cross sections were cut in an RMC ultramicrotome, 1 mm distal to the posterior pole of the eye, collected on gelatin-coated slides, stained with toluidine blue, mounted with Polybed 812 resin, and imaged under an Axioscop 2 Plus microscope (Carl Zeiss). For quantitative analyses, four images at 100× magnification were taken systematically from the cross sections of each nerve. Images of blinded experimental groups were processed with ImageJ software (National Institutes of Health, Bethesda, MD, USA), and the number of myelinated fibers was manually counted by the same person (CAA).

Statistical Treatment. Statistical analyses were performed using GraphPad Prism 8.0 software (GraphPad Software, La Jolla, CA, USA). Data are expressed as mean ± SEM. *P* values less than 0.05 were considered statistically significant. The tests applied, as required for each experiment, are indicated in the legend of each figure.

Results

rAAV2-*MAX* Protects RGCs Ex Vivo

Overexpression of MAX was driven by the ubiquitous promoter cytomegalovirus (CMV)/CBA after intravitreal injection of rAAV2 in neonatal rats, as previously described.[40] Here, we first assessed the effect of overexpressed MAX on RGC survival ex vivo in cultures of retinal explants. One-day-old Lister Hooded rat pups received intravitreal injection of 1 µL rAAV2 at 10^9 vg carrying either human *MAX* transgene or the *GFP* gene as a control. At 14 days after injection of rAAV2, explants of the retinas were maintained ex vivo for 30 hours in free-floating culture. Previously, we showed that axotomy through explantation leads to the death of essentially all ganglion cells over time ex vivo, reaching the maximum rate of cell death at 36 to 48 hours,[40] whereas the amacrine cell population is mostly spared.[51,52] First, we used neutral red staining to identify pyknotic nuclei,[53] which signals the end stage of cell death (Figs. 1A–C). After 30 hours ex vivo, the RGC layer of rAAV2-*GFP*–treated retina contained an average of 44.29% pyknotic nuclei while the average fraction of pyknotic nuclei in retinas treated with rAAV2-*MAX* was significantly decreased to 24.32% (Fig. 1D). In order to correlate MAX expression with cell death in the RGC layer, we double-stained the retinal explants with anti-MAX and TUNEL. After 30 hours ex vivo, we found a reduction of TUNEL labeling from 51.4% in rAAV2-*GFP* to 20% in rAAV2-*MAX*–treated retinas (Fig. 1E; Supplementary Fig. S1), thus confirming the protection of RGCs by rAAV2-*MAX*. The frequency of TUNEL-positive cells in both rAAV2-*GFP*–

Investigative Ophthalmology & Visual Science

Downloaded from hwmaint.iovs.org on 04/25/2024

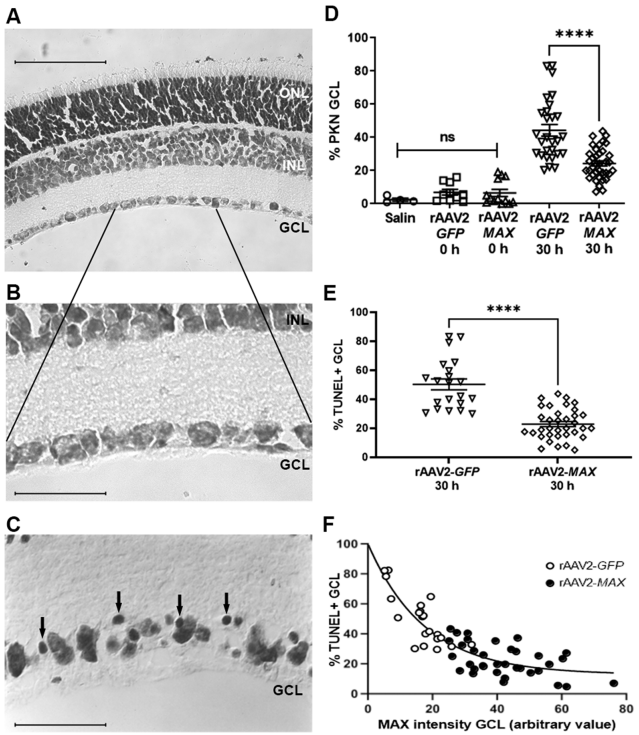

Figure 1. Overexpression of MAX maintains RGC ex vivo. (**A**) Representative section of control retina explant stained with neutral red. *Scale bar*: 300 µm. (**B**) Close-up view of RGC layer. *Scale bar*: 100 µm. (**C**) Representative section of retinal explant after 30 hours ex vivo stained with neutral red. *Arrows* depict pyknotic nucleus. *Scale bar*: 100 µm. (**D**) Graphic depicts percentage of pyknotic nuclei in the RGC layer of explant slices in each experimental group. rAAV2-*MAX* 30 hours is statistically different from rAAV2-*GFP* 30 hours (44.29 ± 3.475 and 24.32 ± 1.56, respectively). Each group represents the mean ± SEM. Statistical analyses were performed with one-way ANOVA plus Holm-Sídak's multiple comparison posttest. ****$P < 0.0001$. (**E**) Comparison of TUNEL staining percentage in the RGC layer of explant slices after 30 hours ex vivo in each experimental group (rAAV2-*GFP* 30 hours: 50.32 ± 3747; rAAV2-*MAX* 30 hours: 22.9 ± 1.79). Each group represents the mean ± SEM. Statistical analyses were performed with parametric *t*-test plus Mann–Whitney posttest. ****$P < 0.0001$. (**F**) Graphic depiction of the correlation between percentage of TUNEL stained and MAX intensity into the RGC layer in slices of retina explants after 30 hours ex vivo in which eyes were intravitreally injected with either rAAV2-*GFP* or rAAV2-*MAX*. GCL, ganglion cell layer; INL, inner nuclear layer; ONL, outer nuclear layer; rAAV2, recombinant adeno-associated virus serotype 2.

and rAAV2-*MAX*–treated explants inversely correlated with the intensity of MAX immunostaining (Fig. 1F), and the data best fit a single-phase exponential decay model (see Supplementary Table S1).

Both the percentage of pyknotic nuclei and that of TUNEL-labeled cells in rAAV2-*GFP*–treated tissue are consistent with the approximate 50% of RGCs resident in the RGC layer of Lister Hooded rats, whereas the remaining half belongs mostly to displaced amacrine cells not directly damaged by the explantation.[51] These ex vivo results suggested that overexpression of MAX protects RGCs from apoptosis induced by axon injury upon retinal explantation.

MAX Overexpression Induced by rAAV2-*MAX* In Vivo

Having ascertained that MAX overexpression prevented death from axotomy of RGCs ex vivo, we next examined

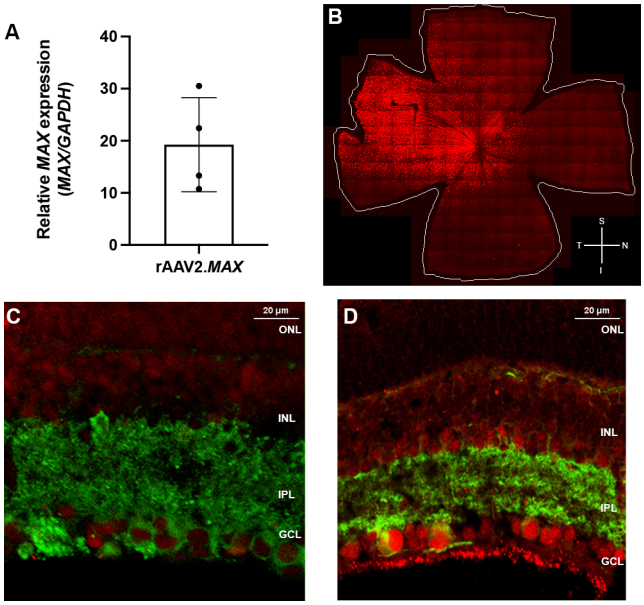

Figure 2. Profile of MAX overexpression in retinas 1 month after intravitreal injection of rAAV2 in adult rat. (**A**) Graph depicts the relative expression of MAX mRNA in four retinas after intravitreal injection compared with the endogenous MAX mRNA of control retinas obtained with quantitative RT-PCR. (**B**) Reconstructed retinal flat-mount image of the RGC layer of injected retina immunostained with anti-Max antibody. I, inferior; N, nasal; S, superior; T, temporal. Colocalization of MAX (*red*) with TUJ-1–positive (*green*) ganglion cells in retinal sections of noninjected eye (**C**) and 1 month after intravitreal injection of rAAV2-*MAX* (**D**). *Scale bar*: 20 µm.

whether rAAV2-*MAX* was neuroprotective in vivo. Initially, we assessed the overexpression of MAX in the retina 30 days after intravitreal injection in young adult rats of 3 µL rAAV2 vector at 10^9 vg/µL. The relative amount of *MAX* mRNA in the entire retinal tissue reached from 10- to 30-fold as compared with endogenous *MAX* in untreated retinas (Fig. 2A). Immunolabeling showed that the injection of rAAV-*MAX* increased the level of MAX protein, mostly at the temporal-superior quadrant, which is the closest to the injection site, covering roughly one-third of the area of the rat retina (Fig. 2B) and particularly intense in the RGC layer (Figs. 2C, 2D). As expected for an rAAV2 vector, increased MAX was detected in RGCs of a wide variety of nuclear sizes (Supplementary Figs. S2A, S2B) and persisted for at least 11 months after the injection (Supplementary Figs. S2C, S2D).

rAAV2-*MAX* Protects RGCs From Degeneration Induced by Optic Nerve Crush

The effect of MAX overexpression was then analyzed after ONC, a classic model of in vivo RGC injury. First, RGCs were retrogradely labeled with DiI injected bilaterally into the superior colliculus of 5-day-old rats. At 1 month of age, the rats were subject to an intravitreal injection of 3 µL of either rAAV2-*MAX* or rAAV2-*GFP* (10^9 vg/µL). Four weeks later, the rats were subject to unilateral ONC, and after additional 2 weeks, we detected a loss of 50% of RGCs (Figs. 3A, 3B, 3D). Overexpression of *GFP* had no effect (Fig. 3D), but in contrast, the density of RGCs following overexpression of MAX was not significantly different from the control retinas (Figs. 3C, D). Importantly, no adverse response was found in the RGCs to either vector injection

Investigative Ophthalmology & Visual Science

Downloaded from hwmaint.iovs.org on 04/25/2024

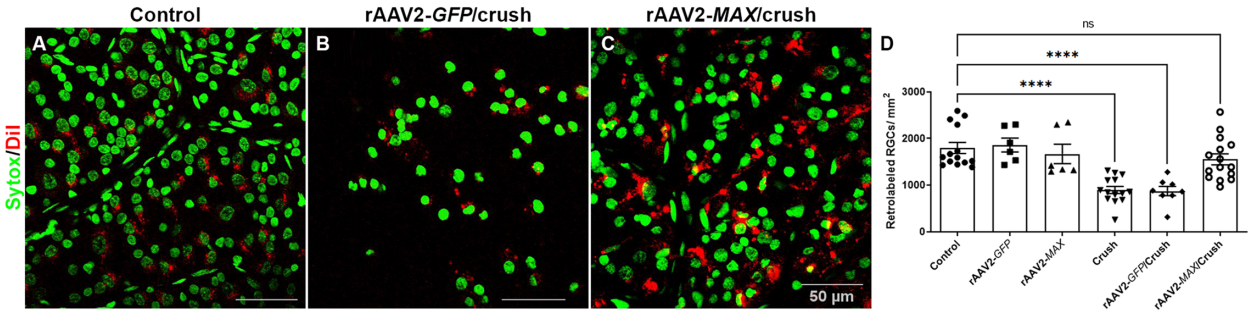

Figure 3. Overexpression of MAX maintains RGCs in vivo after optic nerve crush. (**A–C**) Representative photomicrographs of the RGC layer in flat-mount retinas of different experimental groups stained with DNA-intercalating Sytox Green and DiI (*red*)–positive RGC. *Scale bar*: 50 µm. (**D**) Graph depicts the amount of DiI-retrolabeled RGCs in each experimental group. rAAV2-*GFP* or *MAX* did not alter the amount of unlesioned RGCs. Crush decreased the amount of RGCs in noninjected and rAAV2-*GFP* retinas, while rAAV2-*MAX* preserved RGCs. Each *bar graph* represents the mean ± SEM. Statistical analyses were performed with one-Way ANOVA plus Holm-Sídak's multiple comparisons test. ****$P < 0.0001$. Experimental groups in **D**: control ($n = 14$; 1797 ± 117.8 cells); rAAV2-*GFP* ($n = 6$; 1860 ± 149.9 cells); rAAV2-*MAX* ($n = 6$; 1669 ± 207.3 cells); crush ($n = 14$; 896.4 ± 76.74 cells); rAAV2-*GFP*/crush ($n = 8$; 874 ± 99.14 cells); rAAV2-*MAX*/crush ($n = 15$; 1554 ± 117.4 cells).

or overexpression of the transgenes in unlesioned RGCs (Fig. 3D).

rAAV2-*MAX* Is Neuroprotective in an OHT Rat Model of Glaucoma

To test for neuroprotection in an experimental setting more akin to human glaucoma, we examined the effects of MAX overexpression in a model of subacute OHT, produced by limbal plexus cautery in rats.[44] One-month-old rats received intravitreal injections of 3 µL rAAV2-*MAX* or rAAV2-*GFP* (10^9 vg/µL) and were subject to OHT 1 month later. Increased IOP, typically observed between D1 and D5 in this model, was not altered by either injection of rAAV2 or overexpression of the transgene and progressively returned to normal values at D7 (see Supplementary Fig. S3). The effect of increased content of the MAX protein was estimated at 14 days after induction of OHT in flat-mounted retinas immunostained with the POU domain transcription factor Brn3a, which selectively labels RGCs (Figs. 4A–C). OHT reduced by roughly one-third the average density of Brn3a-labeled RGCs as compared with control eyes (Fig. 4B), especially at the superior and temporal quadrants (Fig. 4C and Supplementary Fig. S4). Whereas the expression of the control GFP transgene had no effect upon the loss of RGCs, MAX overexpression prevented RGC loss to a whole retinal average density not significantly different from the control (Fig. 4B). This neuroprotective effect was particularly effective in the temporal and superior quadrants (Fig. 4C), consistent with the higher amount of exogenous MAX following the intravitreal injections (Fig. 2B). Functional responses of RGCs were assessed by PERG. OHT promoted a significant decrease of PERG amplitude over the whole range of examined spatial frequencies, and overexpression of MAX, but not of *GFP*, prevented the reduction of PERG responses (Fig. 4D).

rAAV2-*MAX* Protects Optic Nerve Axons From OHT-Induced Degeneration

We also examined the population of RGC axons at approximately 1 mm from the posterior pole of the eye in transverse semithin sections of the optic nerve stained with toluidine blue (Figs. 5A–D). Control optic nerve axons were of normal aspect, size, and outline (Fig. 5A). Nevertheless, sections from rat optic nerves at 14 days after OHT contained abundant degenerating axons, with detachment and vacuolization of myelin lamellae, as well as thick and prominent glial cell processes among the nerve fibers, accompanied by disorganization of the nerve fascicles and reduced axonal density (Fig. 5B). Similar changes, although less disorganized fascicles, were found in optic nerve fibers of the rAAV2-*GFP*/OHT group (Fig. 5C), while the optic nerves of rAAV2-*MAX*–injected eyes showed higher numbers of fibers with regular outlines, medium and small sizes, compacted in fascicles separated by glial cells processes, as well as fewer degenerated fibers and hypertrophic glial cell processes than in the GFP group (Fig. 5D). Estimates of axon density showed a statistically significant protective effect of MAX overexpression (Fig. 5E).

Discussion

Consistent with our previous finding of diminished nuclear content of MAX as an early event after RGC axotomy, the present results demonstrated a neuroprotective effect of rAAV2-driven overexpression of the *MAX* gene both ex vivo and in two in vivo models of RGC degeneration, which was reflected by the preservation of electrophysiologic responses. The transcription factor *MAX* is part of a network involved in the regulation of approximately 15% of the genome[54] and plays key roles in multiple functions, such as signaling, cell-cycle regulation, DNA replication, protein and RNA biosynthesis, and energy metabolism.[55] The impact of MAX in many biological processes could direct neuroprotection, targeting multiple factors involved in the pathophysiology of the neuronal damage seen in glaucoma and providing a beneficial effect to prevent the degenerative progression of the disease. MAX is highly expressed in the brain, heart, and lungs, suggesting important transcriptional activity,[56] and recently, *MAX* was singled out as the strongest contributor to overall gene transcription among a set of 25 transcription factors expressed in seven areas of the human brain.[39] Our previous studies suggested that low levels of MAX may disturb its pan-transcriptional regulatory activity, possibly as an early and necessary step for the execution of cell death of the RGCs,[40,41] and preliminary data suggest that

Investigative Ophthalmology & Visual Science

Downloaded from hwmaint.iovs.org on 04/25/2024

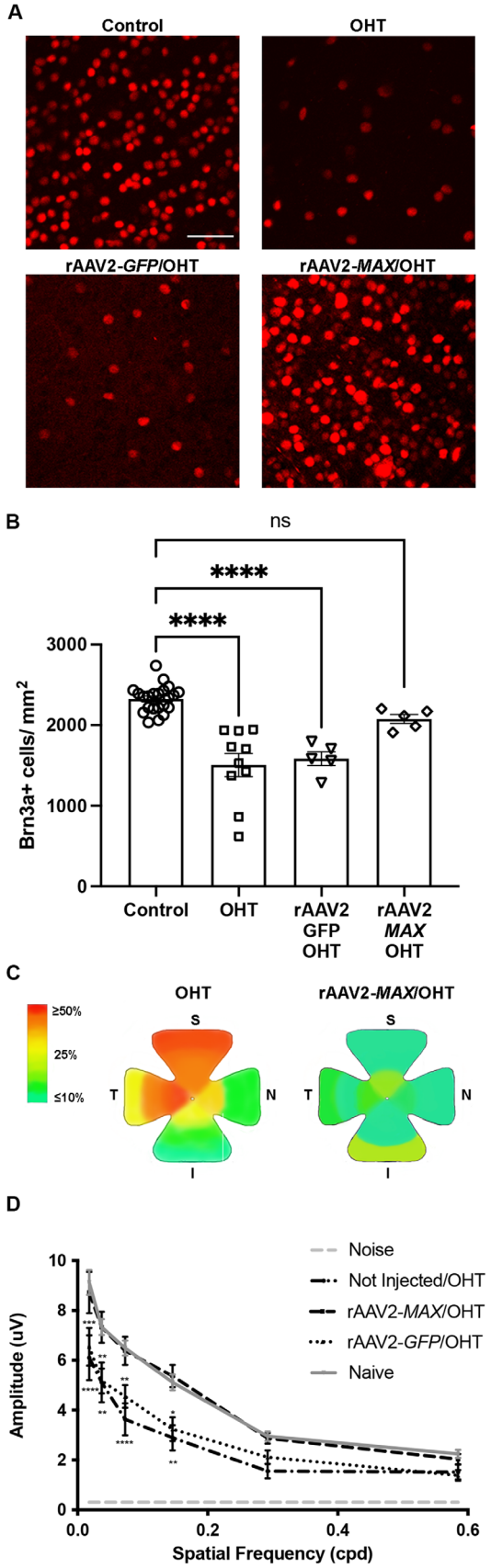

Figure 4. Overexpression of MAX maintains RGCs in vivo after ocular hypertension. (**A**) Representative photomicrographs of BRN3a-immunostained RGC layer in flat-mount retinas of different experimental groups. *Scale bar*: 20 µm. (**B**) Graph depicts the amount of BRN3a-immunostained RGCs in each experimental group. OHT decreased the amount of BRN3a-positive RGCs in noninjected and rAAV2-*GFP* retinas, while rAAV2-*MAX* protected RGCs. Control (n = 22; 2325 ± 35.37 cells); OHT (n = 10; 1506 ± 144.4 cells); rAAV2-*GFP*/OHT (n = 5; 1665 ± 137.1 cells); rAAV2-*MAX*/OHT (n = 5; 2077 ± 56.03 cells). Each bar graph represents the mean ± SEM. Statistical analyses were performed with one-Way ANOVA plus Holm-Sídak's multiple comparisons test. ***P < 0.001, ****P < 0.0001. (**C**) Heatmap illustration representing topographic RGC loss in retinal flat-mount schemes; *left*: noninjected OHT group; *right*: rAAV2-*MAX*/OHT group. I, inferior; N, nasal; S, superior; T, temporal. (**D**) Curves represent PERG amplitudes at different spatial frequencies (mean ± SEM) for each experimental group. Statistical analysis: two-way ANOVA shows both independent variables (spatial frequency and experimental group) are associated with significant changes in PERG amplitudes (*P < 0.1, **P < 0.01, ***P < 0.001, ****P < 0.0001). Holm-Sídak's post hoc test shows that mean PERG amplitudes in the noninjected OHT group and rAAV2-*GFP*/OHT group are statistically different from naive group in 0.018 to 0.292 cycles per degree (cpd) and 0.018 to 0.146 cpd frequencies, respectively, while the rAAV2-*MAX*/OHT group has no statistical difference from the naive group in any spatial frequency evaluated (P > 0.05). Naive (n = 17); noninjected OHT (n = 11); rAAV2-*MAX*/OHT (n = 11); rAAV2-*GFP*/OHT (n = 11).

a widespread network is also controlled by *MAX* both in the normal retina as well as following optic nerve crush (unpublished data). The possibility that MAX decrease is an initial for the execution of cell death is consistent with the current results that MAX overexpression decreases RGC susceptibility regardless of the degeneration trigger, since neuroprotection was shown herein in three distinct RGC insult models.

Core proteins are highly conserved, exert fundamental roles in cells, and therefore are less tolerant to mutations.[57] The MAX protein is highly conserved, with an expected 0.003 amino acid difference per million years.[58] Only a single copy of *MAX* exists in vertebrates despite multiple duplication events, suggesting that the regulation of *MAX* is highly controlled by natural selection.[59] Studies in model organisms such as *Mus musculus*, *Drosophila melanogaster*, and *Caenorhabditis elegans* demonstrate that *MAX* networks maintain functional similarity through extensive evolutionary time, although it has evolved considerably in terms of their sequences, network membership, and complexity.[60] Retention along over a billion years of evolution in such a diverse array of organisms suggests that the *MAX* network has vital roles in cell regulation, organismal development, and its maintenance. This central role for *MAX* is further underlined by the strong phenotype of $MAX^{-/-}$ mice, whose embryos die before day 6.5 of embryogenesis, considerably earlier than animals lacking other members of the Myc family.[38] Recently, MAX was shown to regulate clock gene expression and to contribute to keeping the balance between positive and negative elements of the molecular clock machinery.[61] The circadian clock is a global regulatory mechanism that controls the expression of 50% to 80% of transcripts in mammals.[62] Circadian clock disruption is associated with aging and morbidity.[63] However, much of the evidence linking brain disorders and circadian dysfunction is correlational, and so whether and what kind of causal relationships might exist are unclear. These findings call for in-depth exploration of the therapeutic neuroprotective pathways modulated by overexpression of MAX.

A unique aspect of the data shown here compared with most neuroprotective gene therapies previously used in the

Investigative Ophthalmology & Visual Science

Downloaded from hwmaint.iovs.org on 04/25/2024

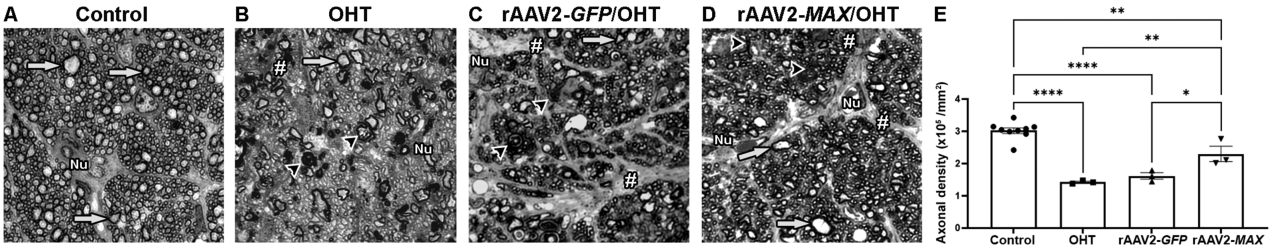

Figure 5. Overexpression of MAX maintains optic nerve structures after ocular hypertension. Representative photomicrographs of semithin optic nerve cross sections stained with toluidine blue from (**A**) control eye, (**B**) 14 days after induction of OHT, (**C**) intravitreally injected with rAAV2-*GFP* and 14 days after OHT, and (**D**) intravitreally injected with rAAV2-*MAX* and 14 days after OHT. *Arrows*: intact morphology of axons; *arrowhead*: degenerative axons; Nu: glial cells nuclei; #: glia cell with hypertrophic processes. *Scale bar*: 7 µm. (**E**) Quantification of optic nerve myelinated fibers shows protection in the axonal fibers in the rAAV2-*MAX*–injected rats compared to other groups. Control ($n = 9$; 3.021 ± 0.08 fibers); OHT ($n = 3$; 1.422 ± 0.029 fibers); rAAV2-*GFP*/OHT ($n = 3$; 1.61 ± 0.1 fibers); rAAV2-*MAX*/OHT ($n = 3$; 2.3 ± 0.23 fibers). Each *bar graph* represents the mean amplitude ± SEM. Statistical analyses were performed with one-way ANOVA plus Holm-Sídak's multiple comparisons test. *$P < 0.05$, **$P < 0.01$, ****$P < 0.0001$.

context of glaucoma and other neurodegenerative conditions is the tumor suppressor role of the transcription factor MAX, of which decreased expression or loss-of-function mutations are related with poor tumor prognosis and tumor formation, respectively.[64,65] Teratogenicity remains a significant issue for applications of gene therapy. Therefore, the coexistence of both a tumor suppressor role and the neuroprotective effects of MAX overexpression is particularly promising for further development of a therapeutic approach to glaucomatous neurodegeneration through gene therapy with the use of rAAV2-*MAX* and/or other similar vectors. To build on the current findings, future studies should test for longer-lasting protective effects of *MAX* gene therapy after RGC injury, its effect in chronic models of glaucomatous neurodegeneration such as the DBA2J mouse, and understanding of the neuroprotective pathways modulated by the overexpression of MAX.

Acknowledgments

The authors thank Jose Nilson dos Santos, Daianne Neves Mandarino Torres, Jose Francisco Tiburcio, and Gildo Brito de Souza at Universidade Federal do Rio de Janeiro for technical support and Robert N. Eisenman (Fred Hutchinson Cancer Research Center, Seattle, WA, USA) for kindly providing *MAX* cDNA.

Supported in part by Coordenação de Aperfeiçoamento de Pessoal de Nível Superior—Brasil (CAPES)—Finance Code 001, Fundação de Amparo à Pesquisa do Estado do Rio de Janeiro (FAPERJ), and Conselho Nacional de Desenvolvimento Científico e Tecnológico (CNPq). This work was also partially supported by Research to Prevent Blindness grant to the Department of Ophthalmology at the University of Florida. Graphical abstract was created with BioRender.com.

Disclosure: **R. Lani-Louzada**, None; **C. Marra**, None; **M.S. Dias**, None; **V.G. de Araújo**, None; **C.A. Abreu**, None; **V.T. Ribas**, None; **D. Adesse**, None; **S. Allodi**, None; **V. Chiodo**, None; **W. Hauswirth**, None; **H. Petrs-Silva**, None; **R. Linden**, None

References

1. Kerrigan LA, Zack DJ, Quigley HA, et al. TUNEL-positive ganglion cells in human primary open-angle glaucoma. *Arch Ophthalmol*. 1997;115:1031–1035.
2. Maddineni P, Kasetti RB, Patel PD, et al. CNS axonal degeneration and transport deficits at the optic nerve head precede structural and functional loss of retinal ganglion cells in a mouse model of glaucoma. *Mol Neurodegener*. 2020;15(1):48.
3. You Y, Gupta VK, Li JC, Klistorner A, Graham SL. Optic neuropathies: characteristic features and mechanisms of retinal ganglion cell loss. *Rev Neurosci*. 2013;24(3):301–321.
4. Calkins DJ, Horner PJ. The cell and molecular biology of glaucoma: axonopathy and the brain. *Invest Ophthalmol Vis Sci*. 2012;53(5):2482–2484.
5. Tezel G. A broad perspective on the molecular regulation of retinal ganglion cell degeneration in glaucoma. *Prog Brain Res*. 2020;256(1):49–77.
6. Pinazo-Durán MD, Zanón-Moreno V, Gallego-Pinazo R, García-Medina JJ. Oxidative stress and mitochondrial failure in the pathogenesis of glaucoma neurodegeneration. *Prog Brain Res*. 2015;220:127–153.
7. Flaxman SR, Bourne RRA, Resnikoff S, et al. Global causes of blindness and distance vision impairment 1990-2020. *Lancet Glob Health*. 2017;5:e1221.
8. Tham YC, Li X, Wong TY, Quigley HA, Aung T, Cheng CY. Global prevalence of glaucoma and projections of glaucoma burden through 2040: a systematic review and meta-analysis. *Ophthalmology*. 2014;121(11):2081–2090.
9. Manifest Glaucoma Trial Group. Reduction of intraocular pressure and glaucoma progression: results from the Early Manifest Glaucoma Trial. *Arch Ophthalmol*. 2002;120:1268–1279.
10. Killer HE, Pircher A. Normal tension glaucoma: review of current understanding and mechanisms of the pathogenesis. *Eye (Lond)*. 2018;32(5):924–930.
11. Tsai JC. Innovative IOP-independent neuroprotection and neuroregeneration strategies in the pipeline for glaucoma. *J Ophthalmol*. 2020;2020:9329310.
12. Jacobson SG, Cideciyan AV, Ho AC, et al. Safety and improved efficacy signals following gene therapy in childhood blindness caused by GUCY2D mutations. *iScience*. 2021;24(5):102409.
13. Askou AL, Jakobsen TS, Corydon TJ. Retinal gene therapy: an eye-opener of the 21st century. *Gene Ther*. 2021;28(5):209–216.
14. Yang Y, Li X, Wang J, et al. A missense mutation in Pitx2 leads to early-onset glaucoma via NRF2-YAP1 axis. *Cell Death Dis*. 2021;12(11):1017.
15. Doucette LP, Rasnitsyn A, Seifi M, Walter MA. The interactions of genes, age, and environment in glaucoma pathogenesis. *Surv Ophthalmol*. 2015;60(4):310–326.
16. Quigley HA, Nickells RW, Kerrigan LA, Pease ME, Thibault DJ, Zack DJ. Retinal ganglion cell death in experimental

Investigative Ophthalmology & Visual Science

Downloaded from hwmaint.iovs.org on 04/25/2024

glaucoma and after axotomy occurs by apoptosis. *Invest Ophthalmol Vis Sci*. 1995;36(5):774–786.

17. Kerrigan LA, Zack DJ, Quigley HA, Smith SD, Pease ME. TUNEL-positive ganglion cells in human primary open-angle glaucoma. *Arch Ophthalmol*. 1997;115(8):1031–1035.
18. Isenmann S, Klöcker N, Gravel C, Bähr M. Short communication: protection of axotomized retinal ganglion cells by adenovirally delivered BDNF in vivo. *Eur J Neurosci*. 1998;10(8):2751–2756.
19. Sapieha PS, Peltier M, Rendahl KG, Manning WC, Di Polo A. Fibroblast growth factor-2 gene delivery stimulates axon growth by adult retinal ganglion cells after acute optic nerve injury. *Mol Cell Neurosci*. 2003;24(3):656–672.
20. Weise J, Isenmann S, Klöcker N, Kügler S, Hirsch S, Gravel C, Bähr M. Adenovirus-mediated expression of ciliary neurotrophic factor (CNTF) rescues axotomized rat retinal ganglion cells but does not support axonal regeneration in vivo. *Neurobiol Dis*. 2000;7(3):212–223.
21. Straten G, Schmeer C, Kretz A, et al. Potential synergistic protection of retinal ganglion cells from axotomy-induced apoptosis by adenoviral administration of glial cell line-derived neurotrophic factor and X-chromosome-linked inhibitor of apoptosis. *Neurobiol Dis*. 2002;11(1):123–133.
22. Takita H, Yoneya S, Gehlbach PL, Duh EJ, Wei LL, Mori K. Retinal neuroprotection against ischemic injury mediated by intraocular gene transfer of pigment epithelium-derived factor. *Invest Ophthalmol Vis Sci*. 2003;44(10):4497–4504.
23. Ghaffariyeh A, Honarpisheh N. Possible pathogenic role of brain-derived neurotrophic factor in glaucoma-like optic neuropathy in patients with intracranial tumours. *Acta Ophthalmol*. 2011;89(5):e475–e476.
24. Schlichtenbrede F, MacNeil A, Bainbridge J, et al. Intraocular gene delivery of ciliary neurotrophic factor results in significant loss of retinal function in normal mice and in the Prph2Rd2/Rd2 model of retinal degeneration. *Gene Ther*. 2003;10:523–527.
25. Lawn S, Krishna N, Pisklakova A, et al. Neurotrophin signaling via TrkB and TrkC receptors promotes the growth of brain tumor-initiating cells. *J Biol Chem*. 2015;290(6):3814–3824.
26. Houck AL, Seddighi S, Driver JA. At the crossroads between neurodegeneration and cancer: a review of overlapping biology and its implications. *Curr Aging Sci*. 2018;11(2):77–89.
27. Planchamp V, Bermel C, Tönges L, et al. BAG1 promotes axonal outgrowth and regeneration in vivo via Raf-1 and reduction of ROCK activity. *Brain*. 2008;131(pt 10):2606–2619.
28. Malik JM, Shevtsova Z, Bähr M, Kügler S. Long-term in vivo inhibition of CNS neurodegeneration by Bcl-XL gene transfer. *Mol Ther*. 2005;11(3):373–381.
29. Kügler S, Klöcker N, Kermer P, Isenmann S, Bähr M. Transduction of axotomized retinal ganglion cells by adenoviral vector administration at the optic nerve stump: an in vivo model system for the inhibition of neuronal apoptotic cell death. *Gene Ther*. 1999;6(10):1759–1767.
30. Krishnan A, Fei F, Jones A, et al. Overexpression of soluble Fas ligand following adeno-associated virus gene therapy prevents retinal ganglion cell death in chronic and acute murine models of glaucoma. *J Immunol*. 2016;197(12):4626–4638.
31. Tirapelli DPDC, Lustosa IL, Menezes SB, et al. High expression of XIAP and Bcl-2 may inhibit programmed cell death in glioblastomas. *Arq Neuropsiquiatr*. 2017;75(12):875–880.
32. Seo J, Park M. Molecular crosstalk between cancer and neurodegenerative diseases. *Cell Mol Life Sci*. 2020;77(14):2659–2680.
33. Bosco A, Anderson SR, Breen KT, et al. Complement C3-targeted gene therapy restricts onset and progression of neurodegeneration in chronic mouse glaucoma. *Mol Ther*. 2018;26(10):2379–2396.
34. Diolaiti D, McFerrin L, Carroll PA, Eisenman RN. Functional interactions among members of the MAX and MLX transcriptional network during oncogenesis. *Biochim Biophys Acta*. 2015;1849(5):484–500.
35. Schaefer IM, Wang Y, Liang CW, et al. MAX inactivation is an early event in GIST development that regulates p16 and cell proliferation. *Nat Commun*. 2017;8:14674–14680.
36. Augert A, Mathsyaraja H, Ibrahim AH, et al. MAX functions as a tumor suppressor and rewires metabolism in small cell lung cancer. *Cancer Cell*. 2020;38(1):97–114.
37. Orian A, van Steensel B, Delrow J, et al. Genomic binding by the Drosophila Myc, Max, Mad/Mnt transcription factor network. *Genes Dev*. 2003;17(9):1101–1114.
38. Shen-Li H, O'Hagan RC, Hou H, Jr, Horner JW, Lee HW, DePinho RA. Essential role for Max in early embryonic growth and development. *Genes Dev*. 2000;14(1):17–22.
39. Hecker N, Seemann SE, Silahtaroglu A, Ruzzo WL, Gorodkin J. Associating transcription factors and conserved RNA structures with gene regulation in the human brain. *Sci Rep*. 2017;7(1):5776.
40. Petrs-Silva H, de Freitas FG, Linden R, Chiarini LB. Early nuclear exclusion of the transcription factor max is associated with retinal ganglion cell death independent of caspase activity. *J Cell Physiol*. 2004;198(2):179–187.
41. Petrs-Silva H, Chiarini LB, Linden R. Nuclear proteasomal degradation and cytoplasmic retention underlie early nuclear exclusion of transcription factor Max upon axon damage. *Exp Neurol*. 2008;213(1):202–209.
42. Shichiri M, Kato H, Doi M, Marumo F, Hirata Y. Induction of max by adrenomedullin and calcitonin gene-related peptide antagonizes endothelial apoptosis. *Mol Endocrinol*. 1999;13(8):1353–1363.
43. Petrs-Silva H, Chiodo V, Chiarini LB, Hauswirth WW, Linden R. Modulation of the expression of the transcription factor Max in rat retinal ganglion cells by a recombinant adeno-associated viral vector [published correction appears in *Braz J Med Biol Res*. 2005;38(6):977]. *Braz J Med Biol Res*. 2005;38(3):375–379.
44. Lani R, Dias MS, Abreu CA, et al. A subacute model of glaucoma based on limbal plexus cautery in pigmented rats. *Sci Rep*. 2019;9(1):16286.
45. Zolotukhin S, Byrne BJ, Mason E, et al. Recombinant adeno-associated virus purification using novel methods improves infectious titer and yield. *Gene Ther*. 1999;6(6):973–985.
46. Zolotukhin S, Potter M, Hauswirth WW, Guy J, Muzyczka N. A "humanized" green fluorescent protein cDNA adapted for high-level expression in mammalian cells. *J Virol*. 1996;70(7):4646–4654.
47. Dias MS, Araujo VG, Vasconcelos T, et al. Retina transduction by rAAV2 after intravitreal injection: comparison between mouse and rat. *Gene Ther*. 2019;26(12):479–490.
48. Harvey AR, Robertson D. Time-course and extent of retinal ganglion cell death following ablation of the superior colliculus in neonatal rats. *J Comp Neurol*. 1992;325(1):83–94.
49. Harvey AR, Cui Q, Robertson D. The effect of cycloheximide and ganglioside GM1 on the viability of retinotectally projecting ganglion cells following ablation of the superior colliculus in neonatal rats. *Eur J Neurosci*. 1994;6(4):550–557.
50. Stabio ME, Sondereker KB, Haghgou SD, et al. A novel map of the mouse eye for orienting retinal topography in anatomical space. *J Comp Neurol*. 2018;526(11):1749–1759.
51. Perry VH. Evidence for an amacrine cell system in the ganglion cell layer of the rat retina. *Neuroscience*. 1981;6(5):931–944.

Investigative Ophthalmology & Visual Science

Downloaded from hwmaint.iovs.org on 04/25/2024

52. Beazley LD, Perry VH, Baker B, Darby JE. An investigation into the role of ganglion cells in the regulation of division and death of other retinal cells. *Brain Res*. 1987;430(2):169–184.
53. Lee Y, McKinnon PJ. Detection of apoptosis in the central nervous system. *Methods Mol Biol*. 2009;559:273–282.
54. Dang CV, O'Donnell KA, Zeller KI, Nguyen T, Osthus RC, Li F. The c-Myc target gene network. *Semin Cancer Biol*. 2006;16(4):253–264.
55. Grandori C, Cowley SM, James LP, Eisenman RN. The Myc/Max/Mad network and the transcriptional control of cell behavior. *Annu Rev Cell Dev Biol*. 2000;16:653–699.
56. Hurlin PJ, Huang J. The MAX-interacting transcription factor network. *Semin Cancer Biol*. 2006;16(4):265–274.
57. Pires-daSilva A, Sommer RJ. The evolution of signalling pathways in animal development. *Nat Rev Genet*. 2003;4(1):39–49.
58. Atchley WR, Fitch WM. Myc and Max: molecular evolution of a family of proto-oncogene products and their dimerization partner. *Proc Natl Acad Sci USA*. 1995;92(22):10217–10221.
59. Young SL, Diolaiti D, Conacci-Sorrell M, Ruiz-Trillo I, Eisenman RN, King N. Premetazoan ancestry of the Myc-Max network. *Mol Biol Evol*. 2011;28(10):2961–2971.
60. McFerrin LG, Atchley WR. Evolution of the Max and Mlx networks in animals. *Genome Biol Evol*. 2011;3:915–937.
61. Blaževitš O, Bolshette N, Vecchio D, et al. MYC-associated factor MAX is a regulator of the circadian clock. *Int J Mol Sci*. 2020;21(7):2294.
62. Doherty CJ, Kay SA. Circadian control of global gene expression patterns. *Annu Rev Genet*. 2010;44:419–444.
63. Lananna BV, Musiek ES. The wrinkling of time: aging, inflammation, oxidative stress, and the circadian clock in neurodegeneration. *Neurobiol Dis*. 2020;139:104832.
64. Augert A, Mathsyaraja H, Ibrahim AH, et al. MAX functions as a tumor suppressor and rewires metabolism in small cell lung cancer. *Cancer Cell*. 2020;38(1):97–114.e7.
65. Mathsyaraja H, Freie B, Cheng PF, et al. Max deletion destabilizes MYC protein and abrogates Eμ-Myc lymphomagenesis. *Genes Dev*. 2019;33(17–18):1252–1264.

Investigative Ophthalmology & Visual Science

Downloaded from hwmaint.iovs.org on 04/25/2024